

# Simulating correlation waveforms of random modulated continuous wave LIDAR

Cibby Pulikkaseril\*

Baraja Pty Ltd., North Ryde, New South Wales, Australia

**Abstract** Advanced light detecting and ranging (LIDAR) sensors are the primary sensing modality for autonomous vehicles and are seeing increasing adoption in consumer and commercial vehicles for robust advanced driver assist systems. LIDAR returns from the environment are typically predicted using elastic LIDAR models, which can help emulate the performance of LIDAR sensors in environments with multiple returns or heavy obscurants. We derive the first elastic LIDAR model for a random modulated continuous wave LIDAR system using a homodyne receiver and show good agreement with experimental measurements. © 2022 Society of Photo-Optical Instrumentation Engineers (SPIE) [DOI: [10.1117/1.OE.62.3.031205](https://doi.org/10.1117/1.OE.62.3.031205)]

**Keywords:** light detecting and ranging; laser ranging; random modulated continuous wave; homodyne detection; light detecting and ranging modeling.

Paper 20220906SS received Aug. 15, 2022; accepted for publication Oct. 5, 2022; published online Nov. 4, 2022.

## 1 Introduction

Light detecting and ranging (LIDAR) sensors are one of the primary sensors used by autonomous vehicles and field robotics, especially when navigating complex, high-speed environments. Although most conventional LIDAR systems use time-of-flight (TOF) or frequency modulated continuous wave architectures for ranging, the use of random modulated continuous wave (RMCW) ranging has seen tremendous interest as it offers high resolution and immunity to interference.

Predicting LIDAR performance through synthesizing LIDAR returns is a thoroughly researched field, as industry and researchers would prefer to use simulated environments for developing autonomous systems rather than collecting enormous amounts of in-field data.<sup>1</sup> Thus, creating a robust emulation of ranging waveform data is an important tool in the use of LIDAR sensors for autonomy and robotic applications. In the simplest case, a single Lambertian target yields a single return with predictable intensity, and this case is easy to predict. However, in realistic environments, the return waveforms are much more complex, as there are partial reflections, impacts of aerosols, beam occlusions, and other effects that complicate the modeling of the return optical signal from the environment.

In this article, we illustrate a novel model for predicting return waveforms for an RMCW LIDAR system and then simulate those returns in a homodyne receiver. In Sec. 2, we extend the typical elastic LIDAR equation, which is usually derived for pulsed TOF LIDAR, to the case of RMCW LIDAR. In Sec. 2, we demonstrate how to use the elastic RMCW return waveform in a homodyne receiver to simulate the received analog signal. Homodyne detection requires a level of complexity because the coherence of the source affects how the detector responds to each range bin, and this analysis demonstrates a robust method of handling these phase delays. Finally, in Sec. 3, we demonstrate the validity of our approach by experimentally creating a complex RMCW return waveform and detect this in a coherent receiver.

### 1.1 Random Modulated Continuous Wave LIDAR

RMCW LIDAR was first proposed by Takeuchi et al.,<sup>2</sup> and referred to the use of intensity and phase modulation of pseudorandom bit sequences to produce unambiguous ranging over a

---

\*Address all correspondence to Cibby Pulikkaseril, [cibby.pulikkaseril@baraja.com](mailto:cibby.pulikkaseril@baraja.com)

defined range. The authors provided an analytical treatment of ranging behavior leading to a definition of signal-to-noise ratio and demonstrated an experimental measurement of the distribution of aerosols over a range of 3 km. Following that work, research into different strains of random sequences, such as A1, A2, and AA1, led to interesting insights into the effect of these modulations on the return waveforms from LIDAR measurements.<sup>3-5</sup> For example, although the sequences were typically designed to minimize background noise, Emery and Flesia concluded that the A1 and A2 sequences could not be used for cloudy conditions.<sup>3</sup>

Homodyne RMCW LIDAR is a natural evolution of the RMCW technique, as achieving shot-noise limited performance increases the link budget of the LIDAR, thereby, increasing the range the LIDAR can detect objects; additionally, the components of a homodyne RMCW LIDAR can be translated, with ingenuity, from optical communications with the homodyne detection of intensity- or phase-modulated signals being used in long-haul networks and referred to as coherent detection.<sup>6</sup> Homodyne RMCW LIDAR has been demonstrated with phase-modulation by Xu et al.<sup>7</sup> The details of demodulating an RMCW signal in a homodyne receiver are discussed by Spollard et al.;<sup>8</sup> they also detail and mitigate the impact of Doppler shifts on the recovery of range information.

## 2 Elastic LIDAR Model for Homodyne RMCW Systems

Our model for an elastic LIDAR that uses RMCW ranging is derived from the work developed for a TOF LIDAR by Phillips et al.,<sup>9</sup> which was developed to consider a sensor in the presence of dust, and to describe several different reporting modes. That model considered the effect of a bistatic TOF LIDAR in an environment with obscurants, such that elastic backscatter provided a return signal to the LIDAR receiver; the range to a target was divided into several range bins that were defined by the transit time of the laser pulse.

In this paper, we reform the elastic LIDAR equations to use an RMCW waveform; this allows us to predict the returned optical power to the LIDAR receiver as a function of time or distance to object. Then, we detect this optical waveform by any receiver architecture that we choose; however, we focus on a single balanced homodyne mixer and predict the impact of multiple returns on the received waveform. In our treatment, however, we ignore the impact of noise sources, and the reader is directed to the analysis by Chen et al.,<sup>10</sup> which provides a good analysis of noise in homodyne receivers.

### 2.1 RMCW Elastic LIDAR Model

A simplified concept of a coaxial RMCW LIDAR is shown in Fig. 1; a laser is modulated with a pseudorandom code, such as a maximum-length sequence (see Takeuchi et al.<sup>2</sup>), and then transmitted through a coaxial transceiver. The transceiver overlaps the transmit and receive beams such that there is perfect alignment of these optical paths at every range location, even as the LIDAR experiences temperature changes or strong vibrations. The transmit beam propagates through the environment, where it may be incident on a variety of objects; most objects in the

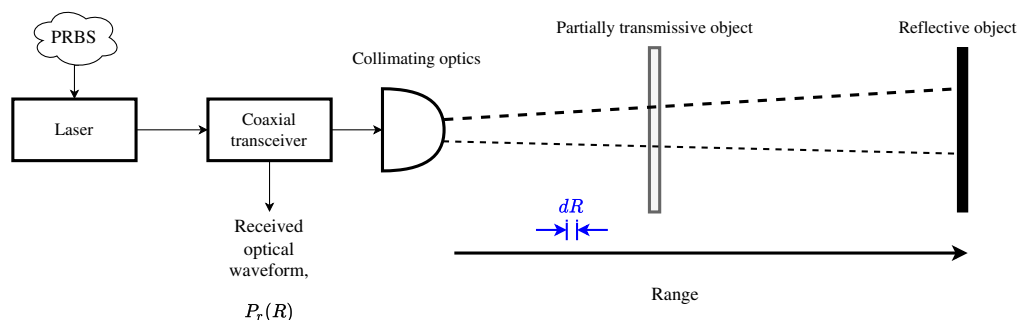


**Fig. 1** A simple schematic of a coaxial LIDAR that emits a beam through a partially transmissive target and then subsequently propagates to a diffuse reflective target.

environment produce a diffuse or Lambertian reflection, whereas in urban environments, we may encounter many specular reflections, such as from metallic surfaces or retroreflective targets, such as traffic signs. One of the motivations for this work is to consider partially transmissive objects, which return some light to the receiver, but let the majority of optical power continue propagating. Examples of these targets are clouds of dust, as derived in Phillips et al.,<sup>9</sup> but also partially transmissive objects such as glass or objects that only obscure part of the beam, such as chain link fences. For the purpose of this analysis, we simply treat all of these objects as a generic partially transmissive object, as shown in Fig. 1.

Using the analysis from Phillips et al. as a reference, we derive the received optical waveform from our coaxial transceiver as  $P_r(R)$ , where each range bin,  $dR$ , represents the slice of distance that corresponds to reflected light from any objects in that differential range width. We consider  $P_r(R)$ , the optical power returned from target at distance  $R$ , to be

$$P_r(R) = P_t(R) * [S_f(R) \cdot D_f(R) \cdot T_f(R)], \quad (1)$$

where  $S_f(R)$  is the fraction of the emitted pulse scattered at range  $R$ ,  $D_f(R)$  is the fraction of the scattered light that is coupled into the LIDAR field-of-view, and  $T_f(R)$  is the fraction of the coupled light that is detected in the receiver.

The scatterable fraction,  $S_f(R)$ , is simply expressed as

$$S_f(R) = \frac{A_S(R)}{A_L(R)}, \quad (2)$$

where  $A_L(R)$  is the spot size, the area illuminated by the transmit beam, and  $A_S(R)$  is the total scattering area from illuminated surfaces. From Phillips et al.,<sup>9</sup> because the authors were predicting LIDAR performance in dust, they counted all particles of dust within one range bin, defined as the length of the optical pulse, and then calculated the scatterable fraction based on the cross-section of each dust particle.

In our approach, we modify this analysis to consider a differential range bin,  $dR$ , and look at the total fraction of light that is scattered from any objects in that range bin with a cross-section of the collimated laser beam. We treat the area of the laser beam as an ellipse with beam waist  $w_y$  and  $w_z$  and define the beam diameter as six times the beam waist, as that captures 99.7% of the intensity in a Gaussian beam. Thus, the area is

$$A_L(R) = 36\pi \cdot w_z w_y. \quad (3)$$

If we consider a uniform cloud of dust, the total area of scattering species is

$$A_S(R) = \sum_i \sigma_i(R), \quad (4)$$

where  $\sigma_i = \pi a^2$  for particles that are spherical with a radius  $a$ . The number of dust particles in the path of the laser beam is

$$n = V \cdot N, \quad (5)$$

where  $N(R)$  is the number density of dust particles in this range bin and  $V$  is the volume containing the  $i$ 'th range bin, which we consider to be a cylinder with height  $dR$ . Thus, we have

$$n = N(R) \cdot 36\pi \cdot w_z w_y \cdot dR. \quad (6)$$

Then, we sum the number of particles to  $n$  as

$$A_S(R) = \sum_{i=1}^n \sigma = n \cdot \sigma = N(R) \cdot 36\pi \cdot w_z w_y \cdot dR \cdot \pi a^2. \quad (7)$$

Thus, we find that the resulting fraction of scattered light is

$$S_f(R) = N(R)\pi a^2 dR. \quad (8)$$

To emulate diffuse targets in the environment, we calculate the scatterable fraction for a Lambertian target, which is usually characterized as having a reflectivity  $\rho$ . In this case, the scatterable fraction at the target distance  $R_T$  is

$$S_f(R = R_T) = 4\pi\rho \cdot dR. \quad (9)$$

The fraction of the scattered light,  $D_f(R)$ , at range  $R$  that returns to the LIDAR receiver is calculated as

$$D_f(R) = \eta \cdot B(R) \cdot O(R), \quad (10)$$

where  $\eta$  is the efficiency of the detector,  $B(R)$  is the fraction of the scattered light that is captured by the FOV of the receiver, and  $O(R)$  is the overlap between the transmit and receive FOV, also known as the LIDAR crossover function.<sup>11</sup>

In our system, we have a coaxial architecture, as shown in Fig. 1, which means that the transmit and receive paths are coincident when propagating from the LIDAR into the environment, and the transceiver separates the receive signal for detection. Although there are disadvantages to a coaxial architecture, one of the major benefits is that the receiver and transmit are always well aligned, even at close distances, because they share the majority of the same optical path—this leads the reader to assume that  $O(R) = 1$  for the coaxial case. In reality, however, the LIDAR optics are designed to maximize returns at the long range and, as a result, the coupling efficiency for targets at short ranges can suffer. In effect, coaxial architectures still experience the equivalent of a crossover function in biaxial LIDAR systems.<sup>11</sup> The analysis of a coaxial crossover function is an interesting area for future work; in this article, we synthesize a crossover function as

$$O(R) = \frac{1}{2}\text{erf}(R/R_C) + \frac{1}{2}, \quad (11)$$

where  $R_C$  is the crossover range in which the system approaches full coupling efficiency and  $\text{erf}(x)$  is the error function.

The perception angle,  $\Omega$ , is the cone projected from the scatterer to the detector lens and is a solid angle of

$$\Omega = \frac{A}{R^2}, \quad (12)$$

where  $A$  is the area of the receiving optics and the solid angle is in steradians. The fraction of the scattered light within the perception angle is

$$B(R) = \frac{1}{4\pi} \cdot \Omega, \quad (13)$$

Then

$$D_f(R) = \frac{1}{4\pi} \cdot \frac{A}{R^2}. \quad (14)$$

Finally, the transmittable fraction,  $T_f(R)$ , is the proportion of light that is available to propagate through the medium. We integrate the losses along the transmitted distance to calculate the reduction in intensity as

$$T(R) = \exp\left[-2 \int_0^R \alpha(r) dr\right], \quad (15)$$

where

$$\alpha(R) = \sum_i (\sigma_{is} + \sigma_{ia}) \cdot n_i(R), \quad (16)$$

where  $\sigma_{is}$  was calculated before as the scattering cross-section.  $\sigma_{ia}$  is the absorption coefficient; this is the energy lost due to water vapor and other absorbing molecules in the atmosphere. In the analysis from Phillips et al.,<sup>9</sup> this is neglected as these effects are considered negligible for IR wavelengths in most environments.

Assembling these components together, we express the final form of our RMCW elastic LIDAR equation. We start with the original expression

$$P_r(R) = P_t(R) * [S_f(R) \cdot D_f(R) \cdot T_f(R)]. \quad (17)$$

Then, we write the final form as

$$P_r(R) = P_t(R) * \left[ (N(R) \cdot \pi a^2 dR) \cdot \left( \frac{1}{4\pi} \cdot \frac{A}{R^2} \right) \cdot \left( \exp \left[ -2 \int_0^R \alpha(r) dr \right] \right) \right]. \quad (18)$$

In a direct-detection system, this power is incident on a photodetector, which is converted to a current/voltage and then digitized. Importantly, the photodetector current is proportional to the optical intensity in a direct-detection scheme. When we analyze the homodyne detection scheme, this square-law relationship gives rise to the beating between the received signal and local oscillator.

To determine the range to targets in the received power waveform, we perform a cross-correlation against the reference transmit waveform. The cross-correlation for the direct-detection case is given as

$$R_{DD}(R) = P_r(R) \star P_t(R), \quad (19)$$

and the identification of targets in the LIDAR return requires peak detection. As we show below, a simple maximum value peak estimation works in simple cases, but the addition of obscurants to the environment can require a more complex peak detection method.

As an example, we calculate the receive optical waveform from a LIDAR that is attempting to detect a target at 200 m, with the line-of-sight obscured by a dust cloud. In this simulated result, we assume a transmit average power of 1 W with an optical aperture diameter of 20 mm. The modulation used on the transmit RMCW waveform is an intensity modulate M-sequence with six registers, resulting in a 63 bit long sequence. In this example, the dust cloud is an idealized dust cloud, from 60 to 70 m, and a number density of 40,000 particles, with each particle having a radius of 50  $\mu\text{m}$ .

The waveforms of transmit and receive are shown in Figs. 2(a) and 2(c), where Eq. (18) is used over every range bin to determine the overall receive optical waveform. The scatterable fraction,  $S_f$ , is shown in log scale in Fig. 2(b), demonstrating the impact of partially transmissive media in the LIDAR path. The return waveform is apparent at 200 m, but it is preceded by a chaotic series of peaks and troughs, which is the impact of a continuous source of backscatter over a range segment. Additionally, we show a plot of  $\log(S_f(R))$ , indicating the scatterable fraction in the environment that returns light to the LIDAR sensor. The factors  $S_f(R)$ ,  $D_f(R)$ , and  $T_f(R)$  are shown as a function of the range in Fig. 3.

In a direct detection system, this received optical signal is converted by a photodetector into an electrical signal, which is digitized by an ADC. The ADC data are then correlated with the original bit sequence used to modulate the laser, which produces peaks at the range in which the targets were detected, assuming that the return signal power is measurable. From the receive optical waveform in Fig. 2(c), the resulting correlation is shown in Fig. 4, with a clear peak at 200 m corresponding to our Lambertian target. Also evident is a distorted peak created by the return optical power from the dust cloud.

In this example, the target peak at 200 m is clearly visible, but the return from the dust cloud has a slightly higher correlation; thus a simple argmax peak estimation algorithm will likely only

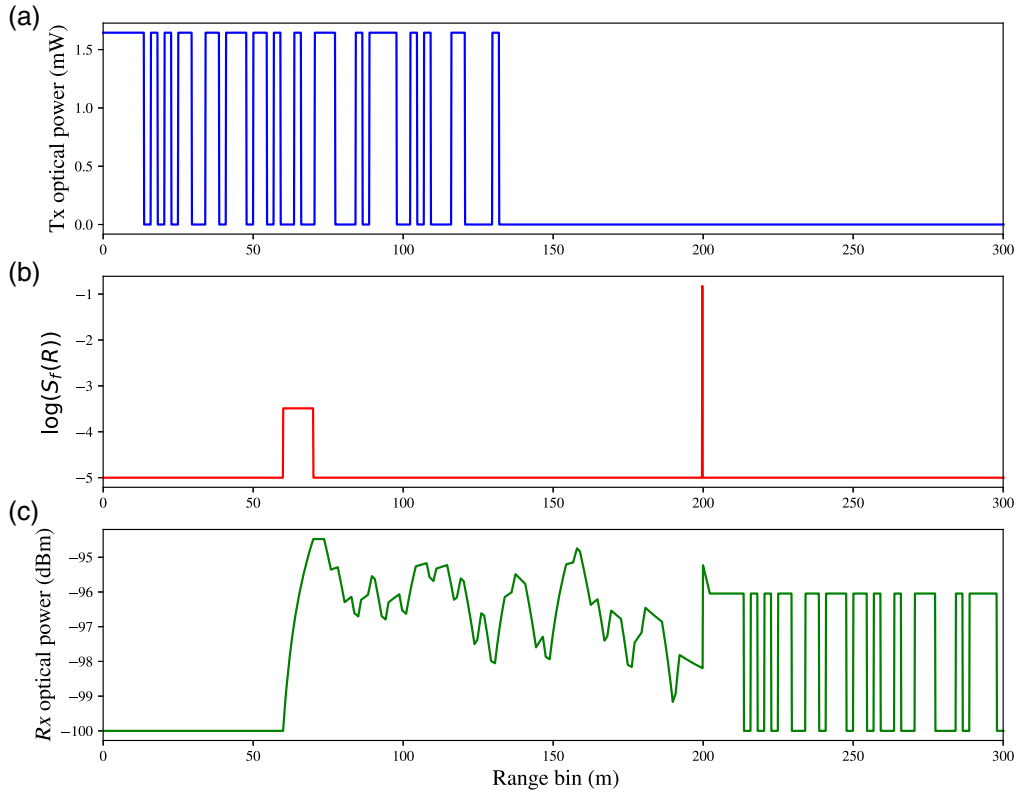


**Fig. 2** Simulated RMCW LIDAR waveform. (a) The transmit ( $T_x$ ) optical waveform is an intensity-modulated  $M$ -sequence; (b) the scatterable fraction plotted over range, showing the dust cloud and the desired target at 200 m; and (c) the received optical waveform received through the LIDAR aperture.

report the dust and ignore the Lambertian target at long range. One of the challenges with any LIDAR system is how to deal with operating in environments with obscitants such as dust; however, as shown here, an RMCW LIDAR does enable the reporting of more information in the environment.

### 2.2 Homodyne Detection of RMCW Waveforms

Homodyne detection is a well-known technique for detecting the amplitude and phase of optical signals,<sup>10</sup> but it requires a more complex receiver, as shown in Fig. 5. the return signal field,  $E_R(t)$ , is mixed with a copy of the original laser waveform, called the local oscillator,  $E_{LO}(t)$ , in a passive optical device called an  $IQ$  demodulator, and balanced photodetectors (BPDs) are used to generate two photocurrents,  $i_{PD,I}(t)$  and  $i_{PD,Q}(t)$ , which are proportional to the  $I$ - and  $Q$ - beat signals from the demodulator. Thus, the square-law relationship of the photodetector enables mixing between the signal and local oscillator fields. A strong treatment of BPDs is given by Alexander,<sup>12</sup> including how balanced detection is used to remove common mode noise. With these two currents, we are able to reconstruct the amplitude and phase of the signal electric field. However, in this article, we only consider the intensity of the signal field to recover the range to targets. A detailed treatment of recovering amplitude and phase, as well as the impact of Doppler shifts on RMCW ranging, is given by Spollard et al.<sup>8</sup>

The BPD receives the sum of the signal and local oscillator fields and has an output photocurrent proportional to the intensity of this total field. Alexander<sup>12</sup> indicates that a single photodiode in the BPD receives a total field of  $E_1(t)$ , given as

$$E_1(t) = \frac{1}{\sqrt{2}} \cdot (E_S(t) + E_{LO}(t)e^{j\pi/2}), \quad (20)$$

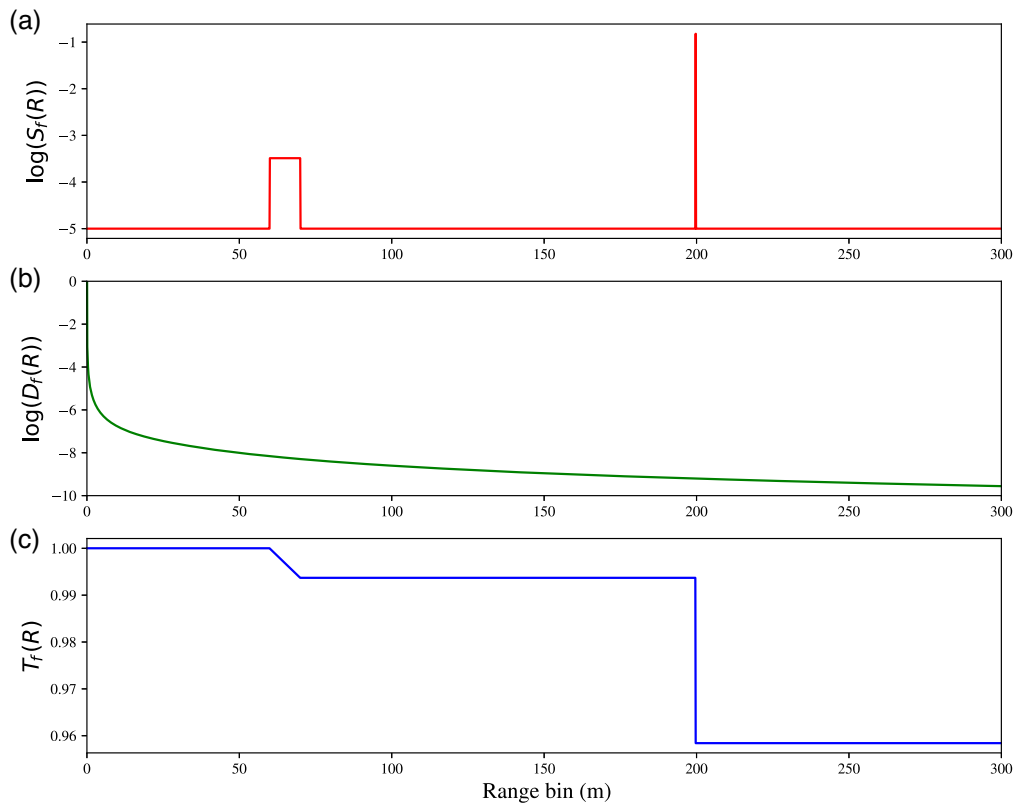


**Fig. 3** The components of the elastic RMCW LIDAR model. (a)  $S_f(R)$  in log scale; (b)  $D_f(R)$  in log scale; and (c)  $T_f(R)$ .

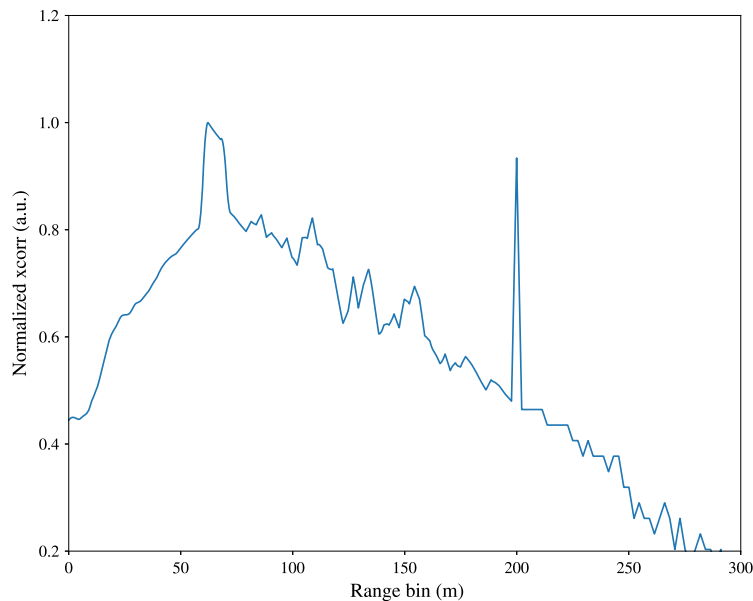


**Fig. 4** Resulting cross-correlation of the received RMCW waveform, where the laser propagates through a dust cloud and then hits a target at 200 m.

where  $E_{LO}(t) = E_{LO} \cdot e^{j\omega_c t + \phi(t)}$  is the local oscillator field, in which  $\omega_c$  is the angular frequency of the lasing wavelength, and  $\phi(t)$  is the time-varying phase of the laser field. Although the phase of the laser field cannot be defined analytically, it can be modeled as a stochastic process with Wiener–Levy statistics.<sup>13</sup>

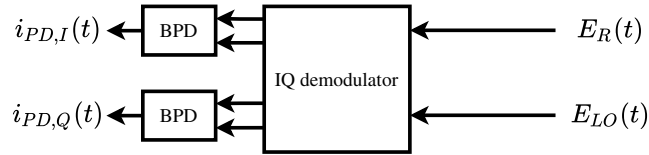


**Fig. 5** In a homodyne receiver, the received electric field,  $E_R(t)$  is fed into one port of an IQ demodulator, and the local oscillator,  $E_{LO}(t)$ , is injected into the second port. The outputs from the demodulator are detected by a BPD and produce currents proportional to the  $I$ - and  $Q$ -beat signals.

To synthesize  $E_S(t)$ , we use the components of Eq. (18) and consider each range bin to be a source of backreflected light, modulated with our  $T_x$  signal, but with amplitude given by the elastic LIDAR equation and time-shifted corresponding to the delay to that range bin,  $T$ . This time-shift delays the modulation, as in the direct detection case, but we must also delay the phase to model a homodyne measurement.

We start by defining a new quantity,  $\gamma_f(R)$ , using the factors of  $S_f(R)$ ,  $D_f(R)$  and  $T_f(R)$ ,

$$\gamma_f(R) = S_f(R) \cdot D_f(R) \cdot T_f(R), \quad (21)$$

which leads us to our model for the received signal field,  $E_R(t)$ :

$$E_R(t) = \sum_i^N \sqrt{\gamma_f(R_i)} \cdot P_i(t - T_i) e^{j\phi(t - T_i)}, \quad (22)$$

where we sum over all  $N$  range bins,  $R_i$  is the  $i$ 'th range bin, and  $R_N$  is the maximum range of our acquisition window. The time-shift,  $T_i$ , is the time delay to the range bin  $R_i$ ; it is used to delay the transmit waveform as well as the optical phase and is given as

$$T_i = \frac{R_i}{2c}, \quad (23)$$

where  $c$  is the speed of light in air.

The currents in the  $I$ - and  $Q$ -branches are given by

$$i_{PD,I}(t) \propto |E_R(t) + E_{LO}(t)|, \quad (24)$$

$$i_{PD,Q}(t) \propto |E_R(t) + jE_{LO}(t)|. \quad (25)$$

With these two quantities, we calculate the received power as the envelope of the combination of the beat signals, given as

$$P_{R,H}(R) = i_{PD,I}^2(t) + i_{PD,Q}^2(t), \quad (26)$$

where we have transformed time into range as  $R = \frac{ct}{2}$ , which results in a homodyne cross-correlation of

$$R_H(R) = P_{R,H}(R) \star P_I(R). \quad (27)$$

### 3 Experimental Setup

To validate the model presented here, we constructed a simple proof-of-concept, as shown in Fig. 6. A semiconductor tunable laser (Lumentum SG-DBR) is used as the source, although it emits a single wavelength of 1545 nm for the purpose of this measurement. The laser output is split into a local oscillator path and a signal path, which we modulate using a lithium niobate Mach-Zehnder modulator (AFR, Zero-Chirp modulator, F10) to intensity modulate a 512-bit

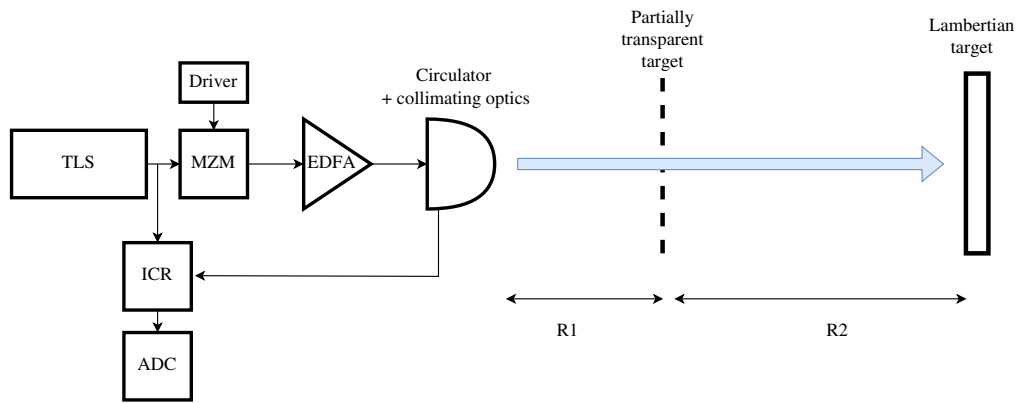


**Fig. 6** Experimental setup: a tunable laser source is intensity modulated with a Mach–Zehnder modulator and amplified with an EDFA. From a single-mode fiber, we transmit into free space using a free-space optical circulator and collimating lens. On the receiver side, we achieve homodyne detection using an ICR and digitize with an ADC.

maximum length sequence on the optical signal. To boost the optical power, we amplify it with an erbium-doped fiber amplifier (EDFA) to achieve a continuous wave power of 30 dBm.

To transmit the RMCW signal into free space, we collimate the beam using a 50-mm aspheric lens. In this specific assembly, the lens was followed by a set of prisms and mirrors used to shape the output beam, but we ignore the effect of these components as it was not relevant to our model. As this is a coaxial system, in which the received light shares the same free-space path as the transmit beam, we use an optical circulator after the EDFA to separate the transmit and receive paths. The light on the receive path is injected into the signal fiber on the intradyne coherent receiver (Neophotonics ICR), which provides phase and polarization diversity, including the photodiodes and the transimpedance amplifiers (TIA). The  $4 \times$  TIA outputs are then digitized by an analog-to-digital converter (ADC) (AD9083).

The collected ADC data are recorded from all outputs of the ICR, but for the purpose of this study, we only consider a single polarization. However, the  $I$  and  $Q$  data from that channel is combined to create a single intensity measurement, which is correlated against the reference modulation. Figure 7 shows the comparison of the measured experimental data after averaging 1000 measurements.

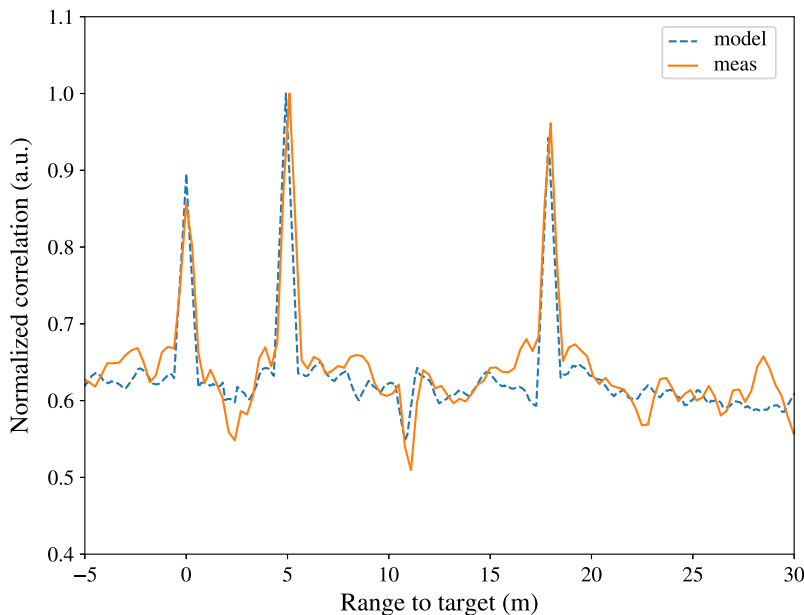


**Fig. 7** Comparison of measured result from a target at 18 m and a mesh screen at 5 m, compared with our predicted model.

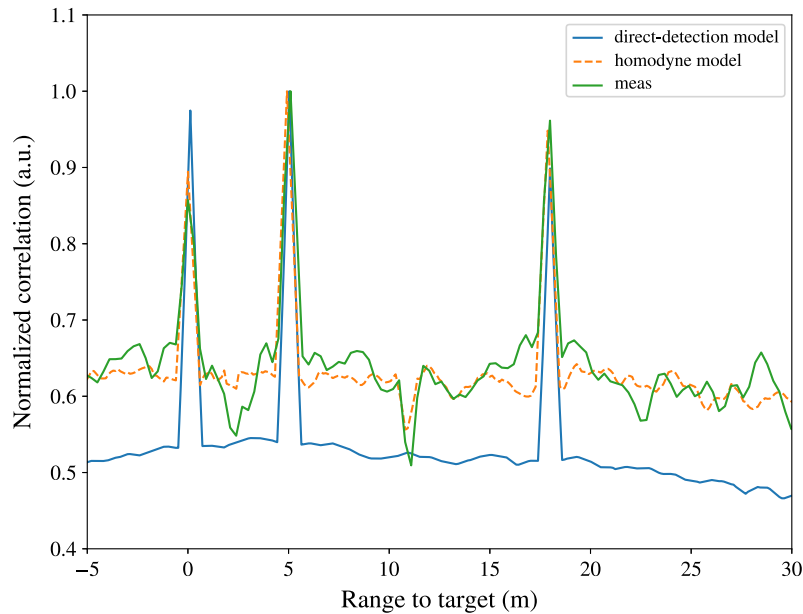


**Fig. 8** Modeling the direct-detection model compared with the homodyne model and the measured result.

The first peak at 0 m is the backreflection from the collimating optics coupling into the receive fiber, and we estimate the backreflection to be 0.0025%. The peak at 5 m is the mesh screen, which is partially transmissive and has a measured reflectivity of 8%, and the peak at 18 m is our 90% Lambertian target. To recover the shape of the correlation, we averaged 1000 measurements, as the correlation floor varies considerably from one measurement to the next.

For our homodyne model, we used a laser linewidth of 30 MHz and Weiner–Levy statistics to generate a random vector of phase values to simulate the optical phase fluctuations. In our creation of  $S_f(R)$ , we used three targets at 0.1, 5, and 18 m, with values of  $\rho$  set as  $5e-5$ , 0.08, and 0.9, respectively.

As we look at the comparison of the model to the measurement result, we see a good agreement, with the exception being the first peak, caused by the backreflection of the collimating lens. The height and shape of the multiple returns is reproduced faithfully, and, interestingly, the notch at 11 m is also predicted. This shows that our model fairly represents the physical system in terms of multiple returns, which is extremely useful in modeling environments with foliage, glass, fences, and other partially transmissive objects.

The figure has been changed to correct for an error in the direct detection case.

In Fig. 8, we show the measurement, the homodyne model, and the equivalent direct detection model with the same parameters. It is clear that the direct detection model can predict the location and width of the target peaks, yet it has poor matching of the waveform outside the peaks. Notably, the homodyne model correctly predicts the local dynamic range of the peaks to the correlation floor. Additionally, the direct detection model does not accurately predict the relative height of the correlation peaks and models much less correlation energy outside the peaks. This demonstrates that a homodyne model is essential to predicting the behavior of these LIDAR systems.

## 4 Conclusion

In this paper, we have derived a model for predicting the received optical waveforms from a homodyne RMCW LIDAR system and have shown how to decode this signal into a correlation function, which is used to disambiguate multiple returns. A simple measurement over 20 m has been completed and compared with the model, which demonstrates good agreement.

Future direction for this work would be to analyze the crossover function,  $O(R)$ , for a coaxial system and include that in the model. Furthermore, measurements over a large set of experimental settings, such as reflectivities and range, particularly long range, would make this model exceptionally valuable for RMCW LIDAR simulation.

## Acknowledgments

The author would like to acknowledge Darcy O'Shea and Dylan Callender for collecting the experimental measurements for this study.

## References

1. S. Manivasagam et al., "LiDARsim: realistic LiDAR simulation by leveraging the real world," in *Proc. IEEE/CVF Conf. Comput. Vis. and Pattern Recognit.*, pp. 11167–11176 (2020).
2. N. Takeuchi et al., "Random modulation CW LiDAR," *Appl. Opt.* **22**(9), 1382–1386 (1983).
3. Y. Emery and C. Flesia, "Use of the A1- and the A2-sequences to modulate continuous-wave pseudorandom noise LiDAR," *Appl. Opt.* **37**(12), 2238–2241 (1998).
4. C. Nagasawa et al., "Random modulation CW LiDAR using new random sequence," *Appl. Opt.* **29**(10), 1466–1470 (1990).
5. A. Rybaltowski and A. Taflove, "Superior signal-to-noise ratio of a new AA1 sequence for random-modulation continuous-wave LiDAR," *Opt. Lett.* **29**(15), 1709–1711 (2004).
6. S. J. Savory et al., "Electronic compensation of chromatic dispersion using a digital coherent receiver," *Opt. Express* **15**(5), 2120–2126 (2007).
7. Z. Xu et al., "Coherent random-modulated continuous-wave LiDAR based on phase-coded subcarrier modulation," *Photonics* **8**(11), 475 (2021).
8. J. T. Spollard et al., "Mitigation of phase noise and Doppler-induced frequency offsets in coherent random amplitude modulated continuous-wave LiDAR," *Opt. Express* **29**(6), 9060–9083 (2021).
9. T. G. Phillips, N. Guenther, and P. R. McAree, "When the dust settles: the four behaviors of LIDAR in the presence of fine airborne particulates," *J. Field Rob.* **34**(5), 985–1009 (2017).
10. Y. Chen et al., "Spectrally balanced detection for optical frequency domain imaging," *Opt. Express* **15**(25), 16390–16399 (2007).
11. K. Sassen and G. C. Dodd, "Lidar crossover function and misalignment effects," *Appl. Opt.* **21**(17), 3162–3165 (1982).
12. S. Alexander, "Design of wide-band optical heterodyne balanced mixer receivers," *J. Lightwave Technol.* **5**(4), 523–537 (1987).
13. M. Tur, B. Moslehi, and J. Goodman, "Theory of laser phase noise in recirculating fiber-optic delay lines," *J. Lightwave Technol.* **3**(1), 20–31 (1985).

**Cibby Pulikkaseril** received his PhD in fiber optic systems at the University of Sydney ('09) and his MEng degree at McGill University ('04). He founded Baraja in 2015 with the concept of using wavelength-tunable lasers and dispersive optics for solid-state beamsteering. Previously, he was the R+D lead at Finisar Australia on optical instrumentation projects, including LCoS programmable processors, and coherent optical spectrum analysis.